Discussion

This study led to three novel findings, as follows. First, we demonstrated a rapid screening system for cell-internalizing mAbs in combination with the phage antibody library, which accelerated the identification of desired cell-internalizing mAbs. Second, comparative *in vivo* studies using cell-internalizing mAbs and low-internalizing mAbs with the same affinity values revealed that mAb internalization contributed to tumor targeting and enhanced the anti-tumor effects of the ADCs. Third, the first *in vivo* therapeutic application with anti-Robo4 mAb revealed that Robo4 is a therapeutic target on the tumor endothelial cells. The first and second findings will greatly contribute to the development of antibody therapies based on cell-internalizing antibodies such as ADCs, targeted liposomal drugs, or imaging. The third finding provides a new focus regarding the role of Robo4 biology in the body; such as the decreased side-effects associated with depleting Robo4-positive endothelial cells *in vivo*.

This method allowed us to successfully isolate anti-Robo4 and anti-VEGFR2 cell-internalizing mAbs in combination with a phage antibody library and a PSIF-based screening system. This method provided one-step screening of cell-internalization of hundreds of "monoclonal" candidates. This is the main advantage of the present system over the old screening system, which required handling a "polyclonal" pool of mAbs[6,7]. The innovative feature of our method is the use of PSIF as a fusion partner for antibodies in scFv format, thus facilitating the identification of antibody fragments capable of efficient internalization. The scFv fusion is much easier than the chemical conjugation of the antibody to a cytotoxic

drug. In principle, this method can be applied to other phage libraries, such as non-immune phage antibody libraries[35,45] or synthetic human phage antibody libraries[46,47], which have already been developed. This system can expand the versatility of phage display systems, which will thus contribute to the development of other cell-internalizing antibodies against various types of antigens for effective cancer therapy.

A comparison of cell-internalizing mAbs with low-internalizing mAbs revealed the strength of the cell-internalizing mAbs in terms of the biodistribution and therapeutic effects. Until now, how internalization contributes to the biodistribution of mAbs has been unclear. In this report, we could use a comparative study to clarify this question because we produced both cell-internalizing mAbs and low-internalizing mAbs with similar binding affinities. As a result, more cell-internalizing mAbs were significantly accumulated in the tumor than low-internalizing mAbs. This is the first evidence to support that mAbs with high internalization activity have greater tumor-targeting potency. This information is also useful for other applications that benefit from cell-internalizing mAbs, such as liposomal drugs, bioactive proteins/peptides, and viral vectors[48,49].

Until now, the usefulness of Robo4-targeted therapy has not been established. Therapy to target VEGF-VEGFR signaling is already common, but the risk of side-effects must be addressed[31-33]. Although VEGFR expression is up-regulated on tumor vessels, it is also observed on the endothelium in healthy tissues. Previous reports also mentioned the toxicity associated with the anti-VEGFR therapies in mouse models [50] and the clinical trial [51]. Therefore, alternative therapies that target tumor angiogenesis are desired. In the present study, we revealed the possibility that

anti-Robo4 ADCs were safer than anti-VEGFR2 ADCs, although they had similar anti-tumor effects. The findings from immunofluorescence and biodistribution studies also support the notion that anti-Robo4 mAbs could accumulate in the tumor without distributing to normal tissues. This is the first finding of Robo4-targeted therapy and suggests that Robo4 is a potential alternative target for tumor vascular targeting. Of course, additional experiments are needed to establish anti-Robo4 as a novel tool in tumor vascular targeting. For example, the pathological observations of normal blood vessels, in-depth toxicological analysis, or the efficacy against other clinical relevant tumor models, are important for the successful story. Such basic analyses regarding Robo4 might accelerate the development of novel medicines that target tumor angiogenesis, including anti-Robo4 ADCs.

Acknowledgments

This study was supported by Grant-in-Aid for Scientific research (B) and Grant-in-Aid for Scientific Research on Innovative Areas from the Ministry of Education, Culture, Sports, Science, and Technology of Japan (MEXT) and the Japan Society for the Promotion of Science (JSPS); Strategic Japanese-Swiss Cooperative Program from Japan Science and Technology Agency (JST) and the Swiss Federal Institute of Technology Zurich (ETHZ).

Authorship Contributions

Y.M. designed the study. M.Y. and Y.T. performed the experiments. Y.M. and M.Y. analyzed the data. Y.M. and M.Y. wrote the initial manuscript. S.T. and Y.T. contributed to the phage display. Y.Y. and N.O. contributed to animal experiments. Y.O., W.C.A., and T.D. contributed to Robo4 related analysis. Y.M. and S.N. were responsible for the overall project. All authors edited the manuscript.

Conflict of Interest Disclosures

The authors declare no competing financial interests.

References

1. Alley SC, Okeley NM, Senter PD. Antibody-drug conjugates: targeted drug delivery for cancer. *Curr Opin Chem Biol.* 2010;14(4):529-537.

2. Isakoff SJ, Baselga J. Trastuzumab-DM1: building a chemotherapy-free road in the treatment of human epidermal growth factor receptor 2-positive breast cancer. *J Clin Oncol.* 2011;29(4):351-354.

3. Ansell SM. Brentuximab vedotin: delivering an antimitotic drug to activated lymphoma cells. *Expert Opin Investig Drugs.* 2011;20(1):99-105.

4. Reichert JM. Antibody-based therapeutics to watch in 2011. *MAbs.* 2011;3(1):76-99.

5. Gerber HP, Senter PD, Grewal IS. Antibody drug-conjugates targeting the tumor vasculature: Current and future developments. *MAbs.* 2009;1(3):247-253.

6. Poul MA, Becerril B, Nielsen UB, Morisson P, Marks JD. Selection of tumor-specific internalizing human antibodies from phage libraries. *J Mol Biol.* 2000;301(5):1149-1161.

7. An F, Drummond DC, Wilson S, et al. Targeted drug delivery to mesothelioma cells using functionally selected internalizing human single-chain antibodies. *Mol Cancer Ther.* 2008;7(3):569-578.

8. Mukai Y, Sugita T, Yamato T, et al. Creation of novel Protein Transduction Domain (PTD) mutants by a phage display-based high-throughput screening system. *Biol Pharm Bull.* 2006;29(8):1570-1574.

9. Chaudhary VK, FitzGerald DJ, Adhya S, Pastan I. Activity of a recombinant fusion protein between transforming growth factor type alpha and Pseudomonas toxin. *Proc Natl Acad Sci U S A.* 1987;84(13):4538-4542.

10. Kreitman RJ, Wilson WH, Bergeron K, et al. Efficacy of the anti-CD22 recombinant immunotoxin BL22 in chemotherapy-resistant hairy-cell leukemia. *N Engl J Med.* 2001;345(4):241-247.

11. Pastan I, FitzGerald D. Pseudomonas exotoxin: chimeric toxins. *J Biol Chem.* 1989;264(26):15157-15160.

12. Legg JA, Herbert JMJ, Clissold P, Bicknell R. Slits and Roundabouts in cancer, tumour angiogenesis and endothelial cell migration. *Angiogenesis.* 2008;11(1):13-21.

13. Huminiecki L, Bicknell R. In silico cloning of novel endothelial-specific

genes. *Genome Res.* 2000;10(11):1796-1806.

14. Huminiecki L, Gorn M, Suchting S, Poulsom R, Bicknell R. Magic roundabout is a new member of the roundabout receptor family that is endothelial specific and expressed at sites of active angiogenesis. *Genomics.* 2002;79(4):547-552.

15. Smith-Berdan S, Nguyen A, Hassanein D, et al. Robo4 cooperates with CXCR4 to specify hematopoietic stem cell localization to bone marrow niches. *Cell Stem Cell.* 2011;8(1):72-83.

16. Park KW, Morrison CM, Sorensen LK, et al. Robo4 is a vascular-specific receptor that inhibits endothelial migration. *Dev Biol.* 2003;261(1):251-267.

17. Seth P, Lin Y, Hanai J, Shivalingappa V, Duyao MP, Sukhatme VP. Magic roundabout, a tumor endothelial marker: expression and signaling. *Biochem Biophys Res Commun.* 2005;332(2):533-541.

18. Okada Y, Yano K, Jin E, et al. A three-kilobase fragment of the human Robo4 promoter directs cell type-specific expression in endothelium. *Circ Res.* 2007;100(12):1712-1722.

19. Okada Y, Jin E, Nikolova-Krstevski V, et al. A GABP-binding element in the Robo4 promoter is necessary for endothelial expression in vivo. *Blood.* 2008;112(6):2336-2339.

20. Jones CA, London NR, Chen H, et al. Robo4 stabilizes the vascular network by inhibiting pathologic angiogenesis and endothelial hyperpermeability. *Nat Med.* 2008;14(4):448-453.

21. Jones CA, Nishiya N, London NR, et al. Slit2-Robo4 signalling promotes vascular stability by blocking Arf6 activity. *Nat Cell Biol.* 2009;11(11):1325-1331.

22. Marlow R, Binnewies M, Sorensen LK, et al. Vascular Robo4 restricts proangiogenic VEGF signaling in breast. *Proc Natl Acad Sci U S A.* 2010;107(23):10520-10525.

23. Koch AW, Mathivet T, Larrivee B, et al. Robo4 maintains vessel integrity and inhibits angiogenesis by interacting with UNC5B. *Dev Cell.* 2011;20(1):33-46.

24. Kerbel RS. Tumor angiogenesis. *N Engl J Med.* 2008;358(19):2039-2049.

25. Paleolog EM. Angiogenesis in rheumatoid arthritis. *Arthritis Res.* 2002;4 Suppl 3:S81-90.

26. Tonnesen MG, Feng X, Clark RA. Angiogenesis in wound healing. *J Investig Dermatol Symp Proc.* 2000;5(1):40-46.

27. Olsson AK, Dimberg A, Kreuger J, Claesson-Welsh L. VEGF receptor signalling - in control of vascular function. *Nat Rev Mol Cell Biol.*

2006;7(5):359-371.

28. Crawford Y, Ferrara N. VEGF inhibition: insights from preclinical and clinical studies. *Cell Tissue Res.* 2009;335(1):261-269.

29. Wicki A, Rochlitz C, Orleth A, et al. Targeting tumor-associated endothelial cells: anti-VEGFR2 immunoliposomes mediate tumor vessel disruption and inhibit tumor growth. *Clin Cancer Res.* 2012;18(2):454-464.

30. Witmer AN, Dai J, Weich HA, Vrensen GF, Schlingemann RO. Expression of vascular endothelial growth factor receptors 1, 2, and 3 in quiescent endothelia. *J Histochem Cytochem.* 2002;50(6):767-777.

31. Kamba T, McDonald DM. Mechanisms of adverse effects of anti-VEGF therapy for cancer. *Br J Cancer.* 2007;96(12):1788-1795.

32. Eremina V, Jefferson JA, Kowalewska J, et al. VEGF inhibition and renal thrombotic microangiopathy. *N Engl J Med.* 2008;358(11):1129-1136.

33. Choueiri TK, Mayer EL, Je Y, et al. Congestive heart failure risk in patients with breast cancer treated with bevacizumab. *J Clin Oncol.* 2011;29(6):632-638.

34. Yoshikawa M, Mukai Y, Okada Y, et al. Ligand-independent assembly of purified soluble magic roundabout (Robo4), a tumor-specific endothelial marker. *Protein Expr Purif.* 2008;61(1):78-82.

35. Imai S, Mukai Y, Nagano K, et al. Quality enhancement of the non-immune phage scFv library to isolate effective antibodies. *Biol Pharm Bull.* 2006;29(7):1325-1330.

36. Yoshikawa M, Mukai Y, Tsunoda S, et al. Modifying the antigen-immunization schedule improves the variety of monoclonal antibodies obtained from immune-phage antibody libraries against HIV-1 Nef and Vif. *J Biosci Bioeng.* 2011;111(5):597-599.

37. Yamamoto Y, Tsutsumi Y, Yoshioka Y, et al. Site-specific PEGylation of a lysine-deficient TNF-alpha with full bioactivity. *Nat Biotechnol.* 2003;21(5):546-552.

38. Hunter WM, Greenwood FC. Preparation of iodine-131 labelled human growth hormone of high specific activity. *Nature.* 1962;194:495-496.

39. Mellman I. Endocytosis and molecular sorting. *Annual Review of Cell and Developmental Biology.* 1996;12:575-625.

40. Holliger P, Hudson PJ. Engineered antibody fragments and the rise of single domains. *Nat Biotechnol.* 2005;23(9):1126-1136.

41. Pavlinkova G, Beresford GW, Booth BJ, Batra SK, Colcher D. Pharmacokinetics and biodistribution of engineered single-chain antibody constructs

of MAb CC49 in colon carcinoma xenografts. *J Nucl Med.* 1999;40(9):1536-1546.

42. Schneider DW, Heitner T, Alicke B, et al. In vivo biodistribution, PET imaging, and tumor accumulation of 86Y- and 111In-antimindin/RG-1, engineered antibody fragments in LNCaP tumor-bearing nude mice. *J Nucl Med.* 2009;50(3):435-443.

43. Maeda H. SMANCS and polymer-conjugated macromolecular drugs: advantages in cancer chemotherapy. *Adv Drug Deliv Rev.* 2001;46(1-3):169-185.

44. Kappen LS, Goldberg IH. Activation and inactivation of neocarzinostatin-induced cleavage of DNA. *Nucleic Acids Res.* 1978;5(8):2959-2967.

45. Okamoto T, Mukai Y, Yoshioka Y, et al. Optimal construction of non-immune scFv phage display libraries from mouse bone marrow and spleen established to select specific scFvs efficiently binding to antigen. *Biochem Biophys Res Commun.* 2004;323(2):583-591.

46. Silacci M, Brack S, Schirru G, et al. Design, construction, and characterization of a large synthetic human antibody phage display library. *Proteomics.* 2005;5(9):2340-2350.

47. Villa A, Lovato V, Bujak E, Wulhfard S, Pasche N, Neri D. A novel synthetic naive human antibody library allows the isolation of antibodies against a new epitope of oncofetal fibronectin. *MAbs.* 2011;3(3):264-272.

48. Sapra P, Allen TM. Internalizing antibodies are necessary for improved therapeutic efficacy of antibody-targeted liposomal drugs. *Cancer Res.* 2002;62(24):7190-7194.

49. Pastan I, Hassan R, Fitzgerald DJ, Kreitman RJ. Immunotoxin therapy of cancer. *Nat Rev Cancer.* 2006;6(7):559-565.

50. Chinnasamy D, Yu Z, Theoret MR, et al. Gene therapy using genetically modified lymphocytes targeting VEGFR-2 inhibits the growth of vascularized syngenic tumors in mice. *J Clin Invest.* 2010;120(11):3953-3968.

51. Nagayama H, Matsumoto K, Isoo N, et al. Gastrointestinal bleeding during anti-angiogenic peptide vaccination in combination with gemcitabine for advanced pancreatic cancer. *Clin J Gastroenterol.* 2010;3(6):307-317.

Table

Table 1 Binding kinetics of antibodies in surface plasmon resonance analysis

antibody	target	format	k_a ($M^{-1}s^{-1}$)	k_d (s^{-1})	K_D (M)
R4-13i	mRobo4	scFv	$1.25 \pm 0.36 \times 10^5$	$5.82 \pm 0.95 \times 10^{-4}$	$5.03 \pm 1.95 \times 10^{-9}$
(internalizing)		dscFv	$1.15 \pm 0.34 \times 10^6$	$5.98 \pm 0.61 \times 10^{-4}$	$5.64 \pm 2.21 \times 10^{-10}$
		IgG	$1.14 \pm 0.55 \times 10^6$	$4.19 \pm 1.70 \times 10^{-4}$	$2.22 \pm 0.51 \times 10^{-10}$
		scFv-PSIF	$7.22 \pm 4.31 \times 10^4$	$4.28 \pm 1.60 \times 10^{-3}$	$6.47 \pm 1.61 \times 10^{-8}$
		IgG-NCS	$1.02 \pm 0.15 \times 10^6$	$4.66 \pm 0.86 \times 10^{-4}$	$4.59 \pm 0.74 \times 10^{-10}$
R4-16	mRobo4	scFv	$1.30 \pm 0.33 \times 10^5$	$5.82 \pm 1.50 \times 10^{-4}$	$4.77 \pm 1.96 \times 10^{-9}$
(low-internalizing)		dscFv	$1.12 \pm 0.03 \times 10^6$	$5.91 \pm 1.50 \times 10^{-4}$	$5.31 \pm 1.96 \times 10^{-10}$
		IgG	$1.06 \pm 0.24 \times 10^6$	$3.60 \pm 0.85 \times 10^{-4}$	$2.76 \pm 0.16 \times 10^{-10}$
		scFv-PSIF	$8.90 \pm 1.42 \times 10^4$	$6.10 \pm 2.45 \times 10^{-3}$	$7.24 \pm 3.74 \times 10^{-8}$
		IgG-NCS	$1.07 \pm 0.12 \times 10^6$	$3.93 \pm 0.54 \times 10^{-4}$	$3.72 \pm 0.89 \times 10^{-10}$
V2-05i	mVEGFR2	scFv	$9.66 \pm 3.57 \times 10^4$	$4.40 \pm 0.95 \times 10^{-4}$	$5.13 \pm 2.61 \times 10^{-9}$
(internalizing)		dscFv	$8.75 \pm 2.03 \times 10^5$	$5.59 \pm 2.57 \times 10^{-4}$	$6.16 \pm 1.47 \times 10^{-10}$
		IgG	$1.14 \pm 0.09 \times 10^6$	$3.21 \pm 0.35 \times 10^{-4}$	$2.84 \pm 0.52 \times 10^{-10}$
		scFv-PSIF	$9.57 \pm 0.84 \times 10^4$	$6.51 \pm 1.87 \times 10^{-3}$	$6.94 \pm 2.63 \times 10^{-8}$
		IgG-NCS	$0.96 \pm 0.06 \times 10^6$	$4.37 \pm 0.90 \times 10^{-4}$	$4.52 \pm 0.79 \times 10^{-10}$
V2-02	mVEGFR2	scFv	$7.94 \pm 1.24 \times 10^4$	$4.28 \pm 3.23 \times 10^{-4}$	$5.07 \pm 3.05 \times 10^{-9}$
(low-internalizing)		dscFv	$8.94 \pm 2.55 \times 10^5$	$5.57 \pm 1.25 \times 10^{-4}$	$6.60 \pm 2.39 \times 10^{-10}$
		IgG	$1.13 \pm 0.22 \times 10^6$	$3.25 \pm 1.10 \times 10^{-4}$	$2.90 \pm 0.98 \times 10^{-10}$
		scFv-PSIF	$9.84 \pm 1.52 \times 10^4$	$5.75 \pm 2.05 \times 10^{-3}$	$5.81 \pm 1.93 \times 10^{-8}$
		IgG-NCS	$1.08 \pm 0.08 \times 10^6$	$5.25 \pm 1.58 \times 10^{-4}$	$4.85 \pm 1.30 \times 10^{-10}$

Binding kinetics were analyzed against mRobo4 (R4-13i and R4-16) or mVEGFR2 (V2-05i and V2-02). Values are shown as means ± s.d. from three different preparations. k_a, association rate constant ($M^{-1}s^{-1}$); k_d, dissociation rate constant (s^{-1}); K_D, equilibrium dissociation constant (k_d / k_a) (M)

Figure legends

Figure 1. Phage display based method to search for cell-internalizing mAbs

The phage antibody library was "enriched" by affinity panning against the desired antigens. Plasmids encoding scFvs were collected from TG1 *E.coli* strains infected by "enriched" phage libraries. Genes of scFvs were digested out and ligated into a PSIF fusion protein expression vector. These plasmids were then transformed to TG1, and then single colonies were picked up. From these individual colonies, monoclonal scFv-PSIF fusions were induced in TG1 supernatants. Using these fusion proteins, binding affinities and internalizing activities of several hundreds of scFv-PSIFs were easily estimated by ELISA and cytotoxicity assays, respectively. Finally, genes of positive scFvs were collected from TG1, and cell-internalizing scFvs were identified by sequencing. In this report, we used anti-Robo4 and anti-VEGFR2 immune phage scFv libraries as the phage antibody libraries, and mRobo4 and mVEGFR2 as the desired antigens.

Figure 2. Screening of cell-internalizing mAbs (ELISA & cytotoxicity assay)

To screen for cell-internalizing mAbs, 315 clones per antigen were analyzed by ELISA and cytotoxicity assay. (a) Result for Robo4, (b) Result for VEGFR2. Monoclonal scfv-PSIFs were induced in TG1 supernatant. The binding properties and cytotoxicities to MS1 cells were then assessed by an ELISA and WST-8 assay, respectively. E; ELISA results, C; WST-8 assay results. Individual results from ELISA (O.D. = 0.8 or 0.5~0.0) and WST-8 assay (cytotoxicity = 30%~0%) were mapped in grayscale densities. The 24 candidates against Robo4 and 17 candidates

against VEGFR2 are indicated by the underline (ELISA O.D. ≥ 0.2 and cytotoxicity ≥ 20%). After omitting redundant clones by sequencing, 1 cell-internalizing mAb and 2 low-internalizing mAbs against mRobo4, and 2 cell-internalizing mAbs and 14 low-internalizing mAbs against mVEGFR2 were identified.

Figure 3. Cell-internalization analyzed by flow cytometry

(a, c) Trypsinization to quantify internalized mAbs. Different forms of $mAbs^{Cy5.5}$ bound to the MS1 cells at 4°C. After washing out the unbound mAbs, internalization was induced for 2 h at 37°C. To detect only internalized mAbs, cell surface proteins were trypsinized. The remaining cellular fluorescence was then analyzed by flow cytometry. (a) Anti-Robo4 $mAbs^{Cy5.5}$, (c) Anti-VEGFR2 $mAbs^{Cy5.5}$. Black; non-trypsinized group, Gray; trypsinized group, White; negative control (anti-His[scFv]$^{Cy5.5}$, anti-His[dscFv]$^{Cy5.5}$ or anti-FLAG[IgG]$^{Cy5.5}$). (b, d) Time course of the internalization. After binding at 4°C, internalization was induced for 0.5, 1, 2, 4, or 8 h at 37°C. The ratio of internalization was calculated using the following formula: internalization (%) = {internalized mAb} / {total bound mAb} × 100 (%) = {(MFI of mAb)$_T$ – (MFI of negative control)$_T$} / {(MFI of mAb)$_N$ – (MFI of negative control)$_N$} × 100 (%). T; trypsinized group, N; non-trypsinized group, MFI; mean fluorescence intensity. (b) Closed and open markers indicate R4-13i and R4-16, respectively. (d) Closed and open markers indicate V2-05i and V2-02, respectively. (b, d) Circle, diamond, and square indicate scFv, dscFv, and IgG, respectively. Each experiment was performed in triplicate. Values are shown as means ± s.d. $^{**}P<0.01$; internalizing mAb versus low-internalizing mAb in each form by 2-way ANOVA (n=3).

Figure 4. *In vivo* tumor targeting activity of cell-internalizing mAbs

(a-d) Biodistribution of dscFvs in B16BL6 tumor-bearing mice. B16BL6 tumor-bearing mice were intravenously administered with (a, c) anti-Robo4 dscFvs^{125I} or (b, d) anti-VEGFR2 dscFvs^{125I}. Each organ was extracted after (a, b) 2 h or (c, d) 24 h, and the radioactivity was measured using a gamma counter. %ID/g tissue was calculated using the following formula: %ID/g tissue = (count/g tissue) / (total injected count) × 100 (%). Tu; tumor, Li; liver, Ki; kidney, Sp; spleen, Lu; lung, He; heart, Br; brain, Bl; blood. (a, c) black; R4-13i[dscFv]^{125I}, gray; R4-16[dscFv]^{125I}, white; anti-His[dscFv]^{125I}. (b, d) black; V2-05i[dscFv]^{125I}, gray; V2-02[dscFv]^{125I}, white; anti-His[dscFv]^{125I}. Values are shown as means ± s.e.m. *P<0.05, **P<0.01, NS; not significant in Student's t test (n=11). (e-s) Co-immunostaining of dscFvs with CD31+ blood endothelial cells on the tissue section. B16BL6 tumor-bearing mice were intravenously administered with dscFvs^{Bio}. The tumor, kidney, and heart were extracted after 2 h. Tissue sections of tumor, kidney, and heart were stained with Streptavidin-PE conjugate. The blood vasculature was also stained with anti-CD31 antibody. Images were digitally merged. Red; dscFv^{Bio}, Green; CD31, Blue; DAPI (nucleus), Yellow; colocalized region of Red and Green. Scale bar represented 100 μm. (e-g) R4-13i[dscFv], (h-j) R4-16[dscFv], (k-m) V2-05i[dscFv], (n-p) V2-02[dscFv] and (q-s) anti-His[dscFv]. (e,h,k,n,q) Tumor section, (f,i,l,o,r) kidney section, and (g,j,m,p,s) heart section.

Figure 5. Enhanced anti-tumor effect of cell-internalizing mAbs

(a-d) Cytotoxicity of scFv-PSIF and IgG-NCS against MS1 cells. MS1 cells were

incubated with serially diluted mAb-drug conjugates for 24 h. Cell viability was then measured using a WST-8 assay. Closed square; internalizing mAbs, open circle; low-internalizing mAbs, open triangle; negative controls. (a) anti-Robo4[scFv]-PSIFs, (b) anti-Robo4[IgG]-NCSes, (c) anti-VEGFR2[scFv]-PSIFs and (d) anti-VEGFR2[IgG]-NCSes. Anti-His[scFv]-PSIF and anti-FLAG[IgG]-NCS were used as negative controls. Values are shown as means ± s.d. (e-h) Anti-tumor effects of scFv-PSIFs or IgG-NCSes. B16BL6 cells were inoculated intracutaneously into C57BL6 mice on day 0. On days 3, 5, 7, 9, and 11, mAb-drug conjugates were intravenously administered (arrow heads). Tumor volume was calculated using the following formula: tumor volume (mm^3) = {major axis of tumor (mm)}×{minor axis of tumor (mm)}^{2}×0.4. Closed square, internalizing mAbs; open circle, low-internalizing mAbs; open triangle, negative controls (anti-His[scFv]-PSIF or anti-FLAG[IgG]-NCS); open diamond, PBS. (e) anti-Robo4[scFv]-PSIFs, (f) anti-Robo4[IgG]-NCSes, (g) anti-VEGFR2[scFv]-PSIFs and (h) anti-VEGFR2[IgG]-NCSes. Values are shown as means ± s.e.m. $^{**}P<0.01$; internalizing mAbs versus low-internalizing mAbs by Bonferroni *post-hoc* analysis with 2-way ANOVA (n=6). (i-l) Change in body weight during therapy experiment. Closed square, internalizing mAbs; open circle, low-internalizing mAbs; open triangle, negative controls (anti-His[scFv]-PSIF or anti-FLAG[IgG]-NCS); open diamond, PBS. (i) anti-Robo4[scFv]-PSIFs, (j) anti-Robo4[IgG]-NCSes, (k) anti-VEGFR2[scFv]-PSIFs and (l) anti-VEGFR2[IgG]-NCSes. Values are shown as means ± s.e.m. $^{**}P<0.01$; internalizing mAbs versus PBS by Bonferroni *post-hoc* analysis with 2-way ANOVA (n=6).

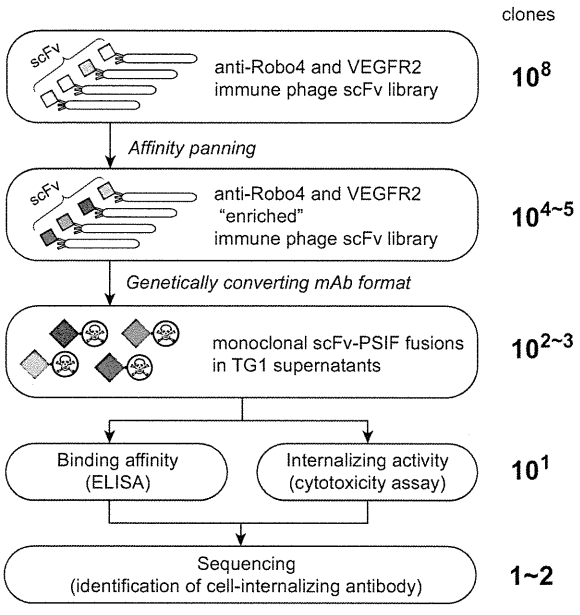

Yoshikawa M et.al.
Figure 1

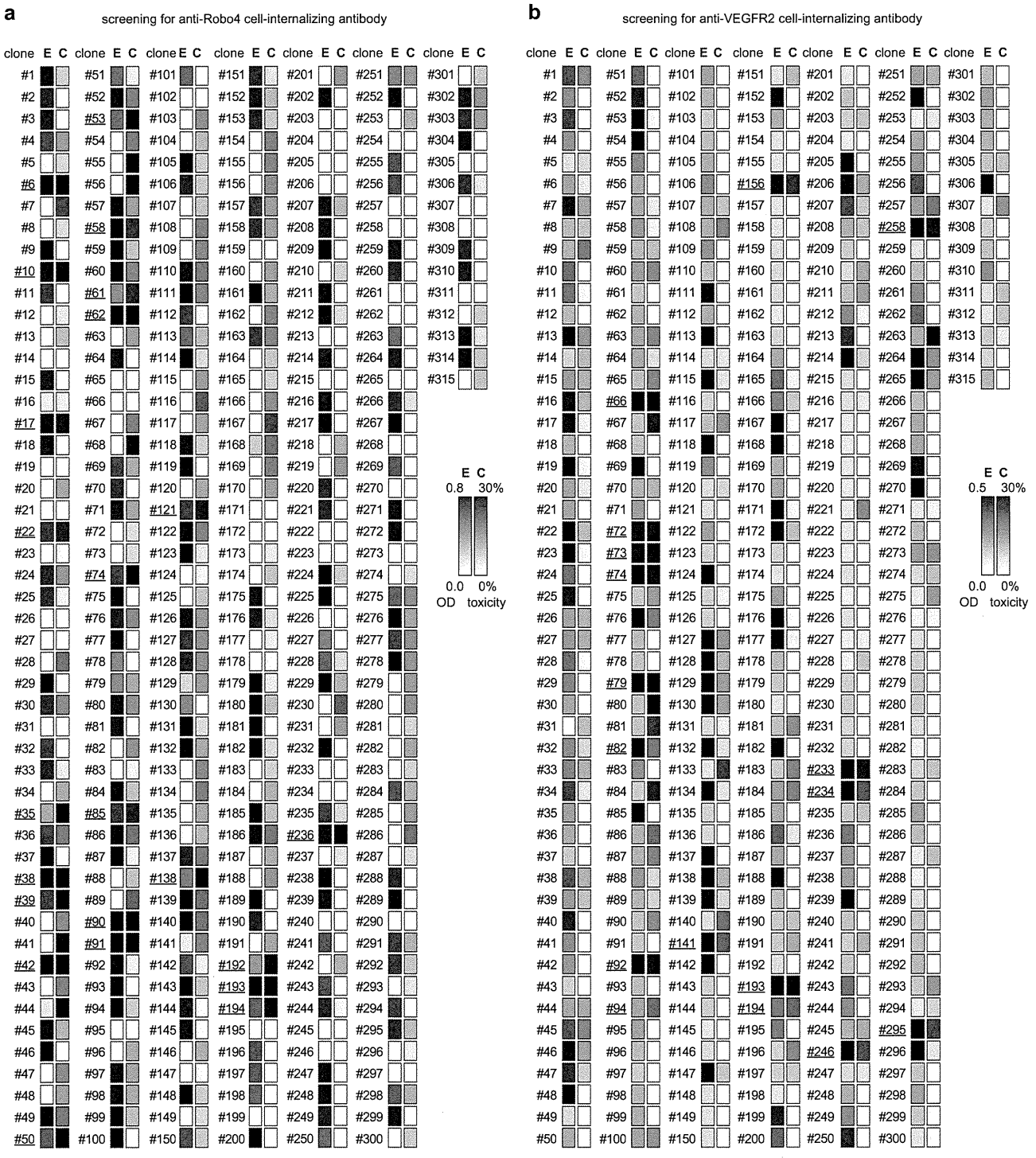

Yoshikawa M et.al.
Figure 2

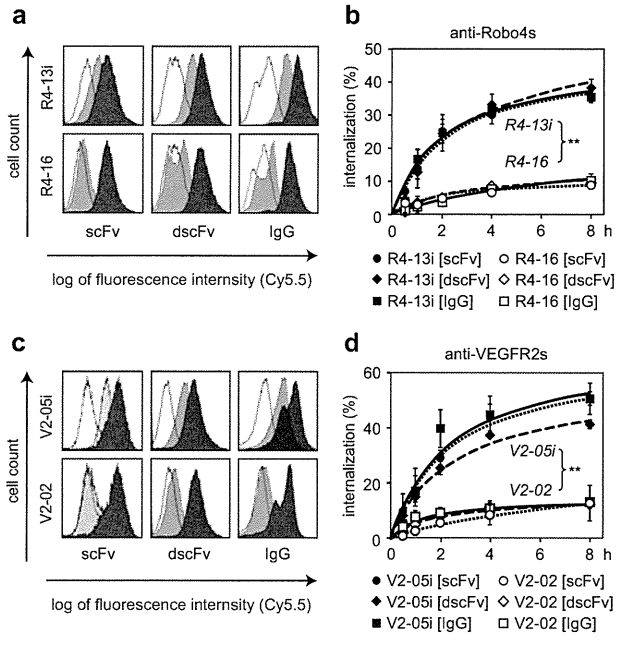

Yoshikawa M et.al.
Figure 3

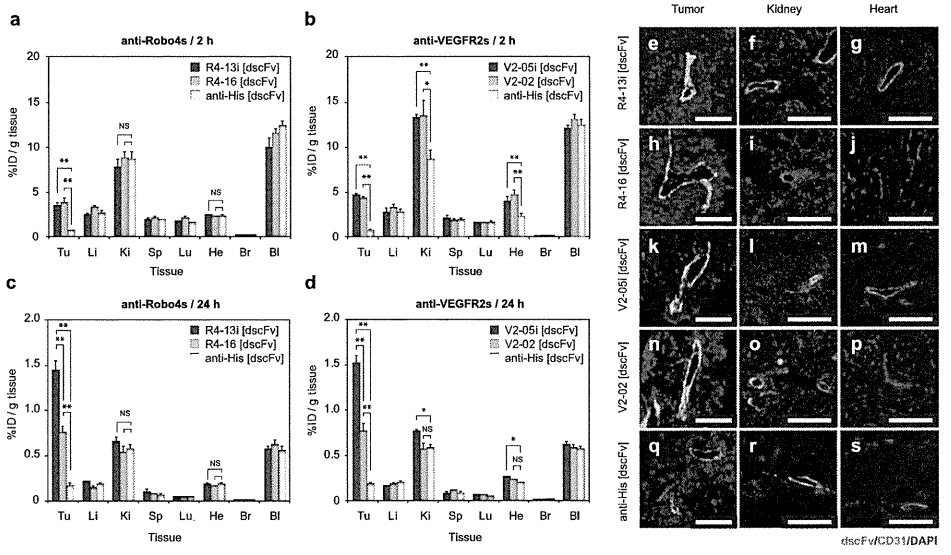

Yoshikawa M et.al.
Figure 4

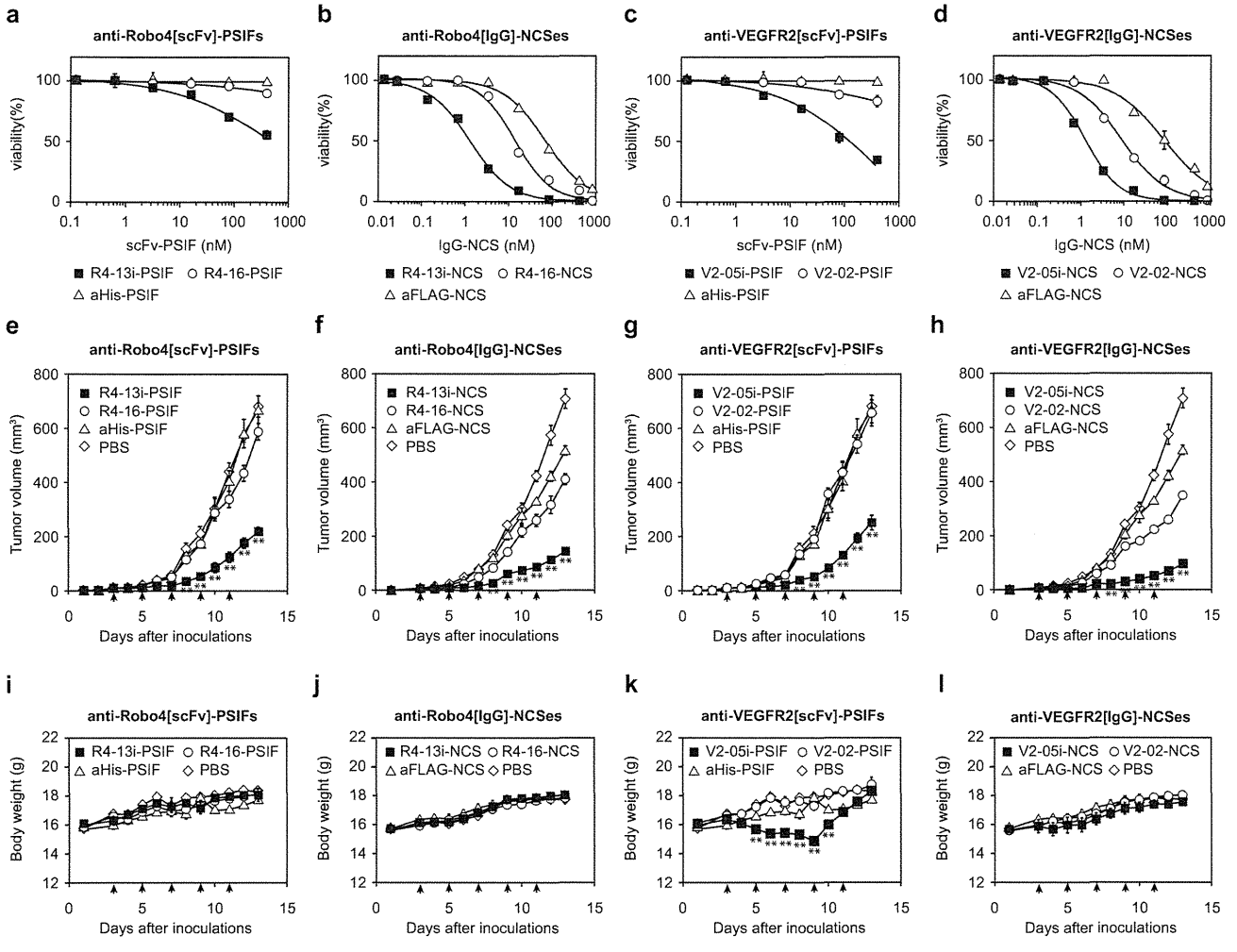

Yoshikawa M et.al.
Figure 5